Comparison of Model-Based Speed Estimation Methods for PMSM Drives

1st Phan Thi Thanh Van
Faculty of Electrical and Electronic Engineering
The University of Danang - University of Technology and Education
Danang, Vietnam
pttvan@ute.udn.vn

2nd Nguyen Anh Tuan
Faculty of Electrical Engineering
The University of Danang - University of Science and Technology
Danang, Vietnam
nguyenanhtuan2410t@gmail.com

3rd Ha Duc Phi
Faculty of Electrical Engineering
The University of Danang - University of Science and Technology
Danang, Vietnam
haducphi246@gmail.com

4th Le Phu Vu
Faculty of Electrical Engineering
The University of Danang - University of Science and Technology
Danang, Vietnam
vulephu.010123@gmail.com

5th Van-Quang-Binh Ngo
Faculty of Physics
University of Education, Hue University
Hue, Vietnam
nvqbinh@hueuni.edu.vn

6th Nguyen Khanh Quang
Faculty of Electrical Engineering
The University of Danang - University of Science and Technology
Danang, Vietnam
nkquang@dut.udn.vn

***Abstract*—This paper presents a unified comparative benchmark of four model-based sensorless speed-estimation algorithms for permanent magnet synchronous motor drives: Luenberger observer (LO), sliding-mode observer (SMO), model reference adaptive system (MRAS), and extended Kalman filter (EKF). The four estimators are implemented under the same PMSM model, operating profile, and simulation conditions. Their performance is evaluated using speed RMSE, position RMSE, steady-state error, maximum transient error, dq-axis current response, THD, disturbance rejection, and implementation complexity. The results show that the EKF achieves the highest estimation accuracy, whereas the SMO provides strong disturbance robustness. The LO and MRAS offer simpler implementation and lower computational cost, although MRAS exhibits larger transient errors. The comparative findings provide practical guidelines for selecting sensorless estimators according to the required trade-off among accuracy, robustness, harmonic behavior, and implementation cost.**

Keywords—PMSM, sensorless control, speed estimation, Luenberger observer, sliding-mode observer, MRAS, extended Kalman filter.

I. INTRODUCTION

Permanent magnet synchronous motors (PMSMs) are increasingly used in electric vehicles, robotic systems, aerospace actuators, and high-performance industrial drives because they combine high efficiency, high power density, and rapid torque response [1]. In these applications, rotor speed and position must be accurately available to implement field-oriented control, regulate torque, and maintain dynamic performance [1], [2]. Although encoders and resolvers can provide this information directly, they increase cost, wiring effort, installation complexity, and maintenance requirements, and they may reduce reliability when the drive operates in harsh environments [1], [3]. Consequently, sensorless speed estimation remains a significant research topic for PMSM drive systems [1]–[3].

Within the broad family of sensorless techniques, model-based estimators are still widely adopted because they use the physical equations of the PMSM to infer speed and position from measured voltages and currents [2], [4]. In comparison with purely data-driven solutions, these approaches are easier to interpret physically, integrate naturally with vector-control schemes, and are more convenient for real-time implementation on embedded drive hardware [2], [5]. Therefore, current PMSM sensorless-control studies continue to improve model-based estimators such as the Luenberger observer (LO), model reference adaptive system (MRAS), sliding-mode observer (SMO), and extended Kalman filter (EKF) [3], [5], [6].

A common basis of many model-based estimators is the reconstruction of back electromotive force (back-EMF) or extended electromotive force (EEMF), from which rotor position and speed can be extracted [2], [4]. This principle is simple and has a clear physical interpretation. However, estimation accuracy may be degraded by parameter errors, noise in current acquisition, inverter nonlinearities, and low-speed operation, where the back-EMF magnitude becomes small [1], [4], [5]. These limitations have motivated the development of more robust observer structures capable of improving accuracy over a wider operating range [5]–[8].

The LO remains an attractive option because of its compact structure and low computational requirement [3], [5]. It estimates the PMSM states by combining the plant model with a feedback correction term, and it usually performs well in medium- and high-speed regions where observability is favorable [3], [5]. Nevertheless, its accuracy depends strongly on model parameters and observer-gain selection, so its robustness may be limited under severe nonlinearities, parameter uncertainties, or abrupt operating changes [3], [5].

The MRAS is also a representative model-based strategy for sensorless PMSM speed estimation [6], [7]. It uses a reference model and a speed-dependent adjustable model, and the speed or position estimate is adapted from the mismatch between their outputs [6]. Its simple structure, straightforward adaptation law, and suitability for real-time implementation make MRAS appealing for practical drives [6], [7]. Recent works have enhanced MRAS through disturbance compensation and nonlinear control mechanisms to improve performance under load and parameter variations [7], [8]. Even with these improvements, MRAS can still be sensitive to low-speed operation and strong model mismatch [6], [7].

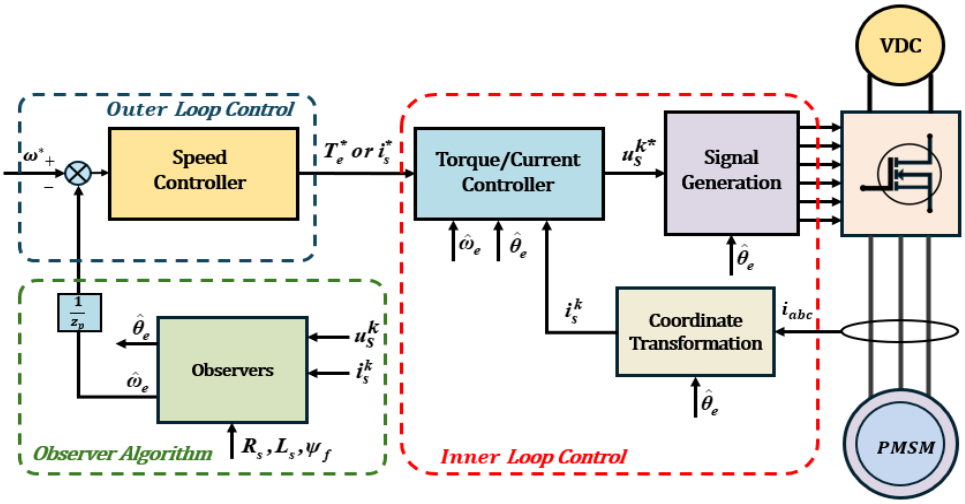

Fig. 1. Sensorless speed PMSM control system

In recent years, the sliding-mode observer has become one of the most active directions in PMSM sensorless control research [8]–[11]. The main advantage of SMO lies in its strong robustness to disturbances, parameter uncertainty, and nonlinear dynamics [8], [9]. For this reason, many recent studies have focused on improved SMO structures, including super-twisting SMO, adaptive SMO, and full-order SMO, with the goal of reducing chattering and improving estimation smoothness while preserving robustness [9]–[11]. These developments have made SMO one of the most competitive model-based methods for modern PMSM drives, especially in applications requiring strong disturbance rejection and stable dynamic performance [8]–[11].

Alongside SMO, the extended Kalman filter and its variants remain among the most theoretically grounded and widely studied approaches for sensorless PMSM estimation [12]–[15]. EKF is attractive because it provides a stochastic state-estimation framework capable of simultaneously reconstructing multiple states in the presence of measurement noise [12], [13]. Recent studies have proposed adaptive EKF, adaptive fading EKF, Runge–Kutta EKF, PS-EKF, and reduced-order EKF structures to improve estimation accuracy while reducing computational burden and enhancing practical implementation feasibility [12]–[15]. These improvements indicate that EKF-based methods continue to play a central role in PMSM sensorless control, particularly when high estimation precision and strong noise-handling capability are required [12]–[15].

Despite the considerable progress achieved by LO-, MRAS-, SMO-, and EKF-based methods, several research gaps still remain. First, many existing methods achieve strong performance only in specific operating regions, such as low-speed, medium-high-speed, or startup conditions, rather than guaranteeing uniformly reliable behavior over the full speed range [1], [5], [8]. Second, higher estimation accuracy is often obtained at the expense of increased structural complexity, heavier computational cost, or more difficult parameter tuning [9], [12], [14]. Third, although the literature on PMSM sensorless control is extensive, relatively fewer studies provide a focused and systematic comparison of model-based sensorless speed estimation methods, particularly among LO, MRAS, SMO, and EKF, using common evaluation criteria such as low-speed observability, robustness to parameter mismatch, disturbance rejection, dynamic response, and implementation cost [2], [3], [5]. Therefore, an updated and structured review of these four representative model-based approaches remains necessary.

The main contribution of this paper is not the proposal of a new observer structure, but a unified and application-oriented benchmark of four representative model-based sensorless estimation methods for PMSM drives. Unlike many previous studies that evaluate each estimator under different models, operating profiles, or performance indicators, this work implements LO, SMO, MRAS, and EKF under the same PMSM model, identical speed/load profiles, and common evaluation criteria. The comparison is extended beyond speed tracking by including rotor-angle estimation, dq-axis current behavior, THD analysis, estimation errors, transient response, disturbance rejection, and implementation complexity. Therefore, the study provides practical guidelines for selecting a suitable estimator according to the required balance among accuracy, robustness, harmonic behavior, and computational cost [1]–[15].

II. Mathematical Model of PMSM Drives

A precise mathematical representation of the PMSM is fundamental for the devlopment of sensorless estimation algorithms. In this study, the motor is modeled in both the stationary $\alpha-\beta$ and the synchronous rotating $d-q$ reference frames to provide the theoretical basis for the observers discussed in the following section.

A. *PMSM Model in the stationary $\alpha-\beta$ frame*

In the stationary $\alpha-\beta$ reference frame, the PMSM can be described in vector form as follows:

$$\begin{cases} u_\alpha = R_s i_\alpha + L_s \dfrac{di_\alpha}{dt} + e_\alpha \\ u_\beta = R_s i_\beta + L_s \dfrac{di_\beta}{dt} + e_\beta \end{cases}, \qquad (1)$$

where u_α, u_β and i_α, i_β are the voltage and current quantities correspond to the $\alpha-$ and $\beta-$ axis stator components; R_s and L_s are the stator resistance and inductance; e_α and e_β represent the back electromotive force (back-EMF), which is expressed as:

$$\begin{cases} e_\alpha = -\omega_e \psi_f \sin\theta_e \\ e_\beta = \omega_e \psi_f \cos\theta_e \end{cases}, \quad (2)$$

in which ω_e and θ_e are the electrical angular speed and electrical rotor position, and ψ_f is the permanent-magnet flux linkage. Since the back-EMF contains speed and position information, it is the key reconstructed variable used by SMO-, EKF-, and LO-based sensorless estimators.

B. PMSM Model in the stationary $d-q$ frame

In the synchronous $d-q$ reference frame, the stator voltage equations are written as:

$$\begin{cases} u_d = R_s i_d + L_d \dfrac{di_d}{dt} - \omega_e L_q i_q \\ u_q = R_s i_q + L_q \dfrac{di_q}{dt} + \omega_e L_d i_d + \omega_e \psi_f \end{cases}, \quad (3)$$

where L_d, L_q are the inductances along the *d*- and *q*-axes.

The MRAS estimator adopted in this work is formulated from the PMSM model in the synchronous $d-q$ frame. Using this model, the estimated currents from the adjustable model are continuously compared with the measured stator currents to obtain the rotor speed estimate [7].

C. PMSM mechanical dynamics

The PMSM has coupled nonlinear electromechanical dynamics. Under vector control, however, the current loop allows the torque relationship to be expressed in a form suitable for observer design and comparison:

$$T_e = \frac{3p\lambda_f}{2} i_q \triangleq K_t i_q. \quad (4)$$

Including the mechanical load, the speed dynamics of the PMSM drive, which are used consistently by the four estimation schemes, are described by:

$$J\frac{d\omega_m}{dt} = T_e - T_L - B\omega_m \quad (5)$$

where T_e is the electromagnetic torque, p is the number of pole pairs, K_t is the torque constant, J is the rotor inertia, B is the viscous damping coefficient, T_L is the load torque, ω_m is the rotor speed.

These integrated models establish a unified mathematical framework for the comparative evaluation of the sensorless strategies investigated in this study.

III. Model Based Methods for Speed Estimation

Figure 1 shows the sensorless PMSM drive considered in this study. The drive includes a voltage source inverter, the PMSM, current controllers, and a speed-estimation block. Instead of using a mechanical speed or position sensor, the controller estimates rotor information from measured stator voltages and currents. Four model-based observers, namely LO, SMO, MRAS, and EKF, are implemented using the unified model introduced in Section II.

A. Sliding Mode Observer (SMO)

The SMO is a nonlinear observer commonly adopted in sensorless PMSM drives because it can maintain estimation performance in the presence of disturbances and parameter variations. Its structure, shown in Fig. 2, is implemented in the stationary $\alpha-\beta$ reference frame and includes a current-estimation model, current-error computation, a discontinuous switching law, and a low-pass filter for extracting the back-EMF. The measured stator currents i_α, i_β are compared with the observer currents $\hat{i}_\alpha, \hat{i}_\beta$, and the resulting error drives the switching action toward the sliding surface [12].

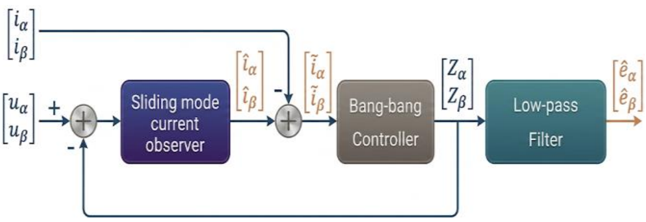

Fig. 2. Structural diagram of the SMO algorithm

From the PMSM model in (1), the current-observer dynamics are written as [7]:

$$\frac{d}{dt}\begin{bmatrix} i_\alpha \\ i_\beta \end{bmatrix} = -\frac{R_s}{L_s}\begin{bmatrix} i_\alpha \\ i_\beta \end{bmatrix} + \frac{1}{L_s}\left(\begin{bmatrix} u_\alpha \\ u_\beta \end{bmatrix} - \begin{bmatrix} e_\alpha \\ e_\beta \end{bmatrix}\right), \quad (6)$$

where e_α and e_β can be expressed by equation (7), which relates to the electrical speed and rotor electrical angle:

$$\begin{bmatrix} e_\alpha \\ e_\beta \end{bmatrix} = \omega_e \psi_f \begin{bmatrix} -\sin\theta_e \\ \cos\theta_e \end{bmatrix} \quad (7)$$

When the back-EMF components in (6) are recovered, rotor speed and electrical angle can be obtained. For this purpose, the sliding-mode current observer is described by:

$$\frac{d}{dt}\begin{bmatrix} \hat{i}_\alpha \\ \hat{i}_\beta \end{bmatrix} = -\frac{R_s}{L_s}\begin{bmatrix} \hat{i}_\alpha \\ \hat{i}_\beta \end{bmatrix} + \frac{1}{L_s}\left(\begin{bmatrix} u_\alpha \\ u_\beta \end{bmatrix} - \begin{bmatrix} z_\alpha \\ z_\beta \end{bmatrix}\right) \quad (8)$$

where $\hat{i}_\alpha$ and $\hat{i}_\beta$ are the estimated stator-current components in the $\alpha-\beta$ frame; and z_α and z_β are the discontinuous switching control terms generated by the bang-bang switching function [8], [9]. The switching vector is defined as:

$$z = \begin{bmatrix} z_\alpha \\ z_\beta \end{bmatrix} = k.\mathrm{sign}\left(\begin{bmatrix} \delta_\alpha \\ \delta_\beta \end{bmatrix}\right), \quad (9)$$

with $\delta^T = \begin{bmatrix} \delta_\alpha & \delta_\beta \end{bmatrix}^T = \begin{bmatrix} (\hat{i}_\alpha - i_\alpha) & (\hat{i}_\beta - i_\beta) \end{bmatrix}^T$ defined as the vector of the difference between the estimated and actual currents. By substituting (6) from (8), the differential error equation can be obtained:

$$\frac{d}{dt}\begin{bmatrix} \delta_\alpha \\ \delta_\beta \end{bmatrix} = -\frac{R_s}{L_s}\begin{bmatrix} \delta_\alpha \\ \delta_\beta \end{bmatrix} + \frac{1}{L_s}\begin{bmatrix} e_\alpha - z_\alpha \\ e_\beta - z_\beta \end{bmatrix}. \quad (10)$$

From equation (9), the tuning coefficient k must be selected such that $\delta^T.\dot{\delta} \le 0$. At this point, $\lim_{t\to\infty} \delta = \lim_{t\to\infty} \dot{\delta} = 0$ and we can estimate the back-EMF through $z = e$. This is verified using Lyapunov stability theory by selecting an appropriate Lyapunov candidate function: $k \geq max\left(\left|e_\alpha\right|.\left|e_\beta\right|\right)$. The issue arises because the $y = sign(x)$ exhibits abrupt value changes between 1 and -1, leading to chattering when the current error δ slides along the sliding surface and approaches zero. To resolve this, two solutions are proposed:

- Replacing the $y = sign(x)$ function with a smoother switching function, specifically the Sigmoid function $y = sigmoid(x)$. This function ensures a smoother output transition by adjusting the coefficient k, and it is less sensitive to noise.

- An LPF is added to attenuate high-frequency components in the estimated back-EMF, as expressed in (11):

$$\hat{e} = \begin{bmatrix} \hat{e}_\alpha \\ \hat{e}_\beta \end{bmatrix} = \frac{\omega_c}{s + \omega_c} \begin{bmatrix} z_\alpha \\ z_\beta \end{bmatrix}, \qquad (11)$$

where ω_c denotes the filter cut-off frequency.

After the back-EMF is obtained from the SMO, the rotor position and speed can be calculated using the arctangent relation:

$$\begin{cases} \hat{\theta}_e = \arctan\left(-\dfrac{\hat{e}_\alpha}{\hat{e}_\beta}\right). \\ \hat{\omega}_e = \dfrac{d\hat{\theta}_e}{dt} \end{cases} \qquad (12)$$

Direct arctangent extraction may introduce speed $\hat{\omega}_e$ and position $\hat{\theta}_e$ ripples when the estimated back-EMF $\hat{e}_\alpha$,$\hat{e}_\beta$ contains harmonic components. Therefore, a phase-locked loop (PLL) is adopted to obtain a smoother position estimate and to mitigate both high-order harmonic noise and chattering effects [7].

B. Luenberger Observer (LO)

The LO is a deterministic state estimation strategy that utilizes a linear feedback correction mechanism to reconstruct the internal states of the PMSM. Unlike stochastic filters, the LO provides a direct approach to state observation by placing the estimator poles in a stable region of the complex plane [5]. The structural framework of the proposed LO for sensorless speed estimation is illustrated in Fig. 3.

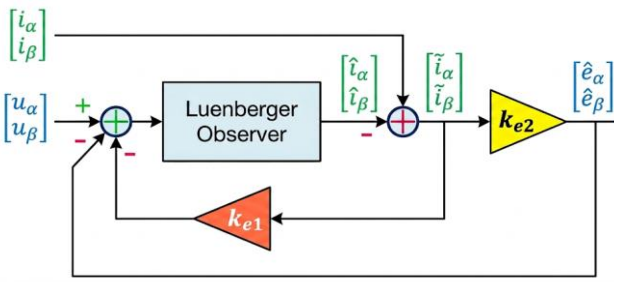

Fig. 3. Structural diagram of the LO algorithm

The proposed LO is composed of two coupled feedback loops driven by the current estimation error, including an inner loop that corrects the current estimation through the gain and an outer loop that reconstructs the back-EMF through the gain.

The observer takes the stator voltage vector $u_{\alpha\beta} = [u_\alpha \quad u_\beta]^T$ and the measured current vector $i_{\alpha\beta} = [i_\alpha \quad i_\beta]^T$ as inputs, and produces the estimated current vector $\hat{i}_{\alpha\beta}$ and estimated back-EMF vector $\hat{e}_{\alpha\beta}$.

The current estimation error is defined as:

$$e_i = i_{\alpha\beta} - \hat{i}_{\alpha\beta} \qquad (13)$$

This error signal simultaneously feeds both feedback loops, which is the key feature distinguishing the LO from conventional observers.

Based on the block diagram in Fig. 3, the observer dynamics can be expressed as:

Current estimation:

$$\begin{cases} \dfrac{d\hat{i}_\alpha}{dt} = \dfrac{1}{L_s}u_\alpha - \dfrac{R_s}{L_s}\hat{i}_\alpha - \dfrac{1}{L_s}\hat{e}_\alpha + k_{e1}\left(i_\alpha - \hat{i}_\alpha\right) \\ \dfrac{d\hat{i}_\beta}{dt} = \dfrac{1}{L_s}u_\beta - \dfrac{R_s}{L_s}\hat{i}_\beta - \dfrac{1}{L_s}\hat{e}_\beta + k_{e1}\left(i_\beta - \hat{i}_\beta\right) \end{cases} \qquad (14)$$

Back-EMF reconstruction:

$$\begin{cases} \hat{e}_\alpha = k_{e2}\left(\hat{i}_\alpha - i_\alpha\right) \\ \hat{e}_\beta = k_{e2}\left(\hat{i}_\beta - i_\beta\right) \end{cases} \qquad (15)$$

It can be observed that the back-EMF is reconstructed directly from the current estimation error through a proportional gain k_{e2}, avoiding the need for discontinuous injection as in the SMO.

The estimated back-EMF components $\hat{e}_\alpha$ and $\hat{e}_\beta$ are then used to compute the estimated rotor electrical angle and electrical angle speed [3]:

$$\hat{\theta}_e = \arctan\left(-\frac{\hat{e}_\alpha}{\hat{e}_\beta}\right) \qquad (16)$$

$$\hat{\omega}_e = \frac{\sqrt{\hat{e}_\alpha{}^2 + \hat{e}_\beta{}^2}}{\psi_f} \qquad (17)$$

Alternatively, a phase-locked loop (PLL) can be employed to improve noise immunity and dynamic performance. The primary challenge in LO design lies in the optimal selection of the gain matrix. While manual tuning provides satisfactory performance at steady-state, advanced metaheuristic algorithms, such as Particle Swarm Optimization (PSO), are increasingly utilized to minimize the estimation error and improve the observer's bandwidth under load torque disturbances [3].

C. Model Reference Adaptive System (MRAS)

The MRAS is a model-based sensorless estimation scheme with a simple computational structure and an explicit adaptation mechanism. It compares a physical reference model with a speed-dependent adjustable model to identify the rotor velocity [6]. As shown in Fig. 4, the implementation used here includes a reference model, an adjustable model, and an

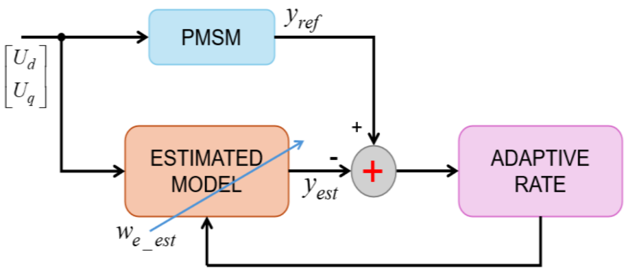

Fig. 4. Structural diagram of the MRAS algorithm

adaptation law, typically realized by a PI controller. The mismatch between the two model outputs is processed by the adaptation law, and the updated speed estimate is fed back to the adjustable model until convergence is achieved.

In the present implementation, the stator-current equations in the synchronous rotating $d-q$ frame are used. The reference model represents the motor dynamics obtained from measurable voltages and currents [1], [4]:

$$\begin{cases} \dfrac{di_d}{dt} = \dfrac{1}{L_d}\left(u_d - R_s i_d + \omega_e L_q i_q\right) \\ \dfrac{di_q}{dt} = \dfrac{1}{L_q}\left(u_q - R_s i_q - \omega_e L_d i_d - \omega_e \psi_f\right) \end{cases} \tag{18}$$

The adjustable model employs the same mathematical structure but replaces the actual electrical speed ω_e with the estimated speed $\hat{\omega}_e$, producing the estimated current states $\hat{i}_d$ and $\hat{i}_q$. The estimation error vector is defined as $\varepsilon = [i_d - \hat{i}_d \quad i_q - \hat{i}_q]^T$. To satisfy Popov's hyperstability condition, the speed-identification law is expressed as [4]:

$$\hat{\omega}_e = \left(K_p + \frac{K_i}{s}\right)\xi \tag{19}$$

where ξ is the generalized error signal derived from the cross-product of the reference and adjustable states. For a non-salient PMSM, this error signal is typically simplified to [5]:

$$\xi = (i_d \hat{i}_q - i_q \hat{i}_d - \frac{\psi_f}{L_s}\left(i_q - \hat{i}_q\right) \tag{20}$$

The rotor electrical position is obtained by integrating the estimated electrical speed:

$$\hat{\theta}_e = \int \hat{\omega}_e \, dt \tag{21}$$

D. Extended Kalman Filter (EKF)

EKF is a recursive nonlinear state estimation method derived from the classical Kalman filter and is widely used in electrical drives to estimate unmeasurable variables such as rotor speed and position. By linearizing the system model at each sampling instant, it can effectively reduce the influence of process disturbances and measurement noise [15].

Figure 5 illustrates the EKF observer structure for the PMSM drive. The algorithm works through prediction and

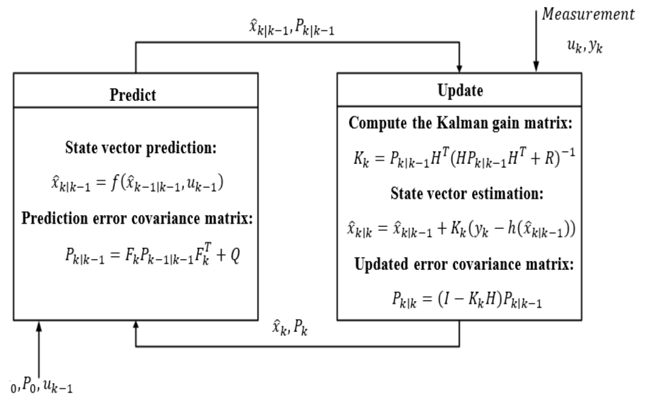

Fig. 5. FStructural diagram of the EKF algorithm

correction stages. During prediction, the nonlinear state model provides an a priori state estimate; during correction, the measured-output residual updates that estimate. This feedback mechanism improves the accuracy of the reconstructed states under model uncertainty and noisy measurements.

The EKF receives stator voltages u_α, u_β and measured currents i_α, i_β and provides the estimated state vector:

$$\hat{x} = [\hat{i}_\alpha \quad \hat{i}_\beta \quad \hat{\omega}_e \quad \hat{\theta}_e]^T \tag{22}$$

This structure ensures closed-loop estimation, where the estimation error is continuously corrected based on measurement residuals.

To implement the EKF, the non-linear PMSM dynamics established in Section II are discretized with sampling period T_s and represented in a state-space form:

$$\begin{cases} x_{k+1} = f(x_k, u_k) + w_k \\ y_{k+1} = h(x_k) + v_k \end{cases} \tag{23}$$

where the state vector is defined as $x_k = [i_\alpha \quad i_\beta \quad \omega_e \quad \theta_e]^T$, the measurement vector is defined as $y_k = [i_\alpha \quad i_\beta]^T$. The vectors w_k and v_k represent the process and measurement noise with covariance matrices Q and R respectively. The non-linear transition function $f\left(x_k, u_k\right)$ is derived from the motor dynamics:

$$f\left(x\right) = \begin{bmatrix} \left(1 - \dfrac{R_s T_s}{L_s}\right) i_\alpha + \dfrac{T_s \psi_f}{L_s} \omega_e \sin\theta_e + \dfrac{T_s}{L_s} u_\alpha \\ \left(1 - \dfrac{R_s T_s}{L_s}\right) i_\beta + \dfrac{T_s \psi_f}{L_s} \omega_e \cos\theta_e + \dfrac{T_s}{L_s} u_\beta \\ \omega_e \\ \theta_e + \omega_e T_s \end{bmatrix} \tag{24}$$

The nonlinear model is linearized around the current estimate using the Jacobian matrix F_k:

$$F_k = \frac{\partial f(x,u)}{\partial x}\Big|_{\hat{x}_{k|k}}$$

$$= \begin{bmatrix} 1-\frac{R_sT_s}{L_s} & 0 & \frac{T_s\psi_f}{L_s}\sin\hat{\theta}_e & \frac{T_s\psi_f}{L_s}\hat{\omega}_e\cos\hat{\theta}_e \\ 0 & 1-\frac{R_sT_s}{L_s} & -\frac{T_s\psi_f}{L_s}\cos\hat{\theta}_e & \frac{T_s\psi_f}{L_s}\hat{\omega}_e\sin\hat{\theta}_e \\ 0 & 0 & 1 & 0 \\ 0 & 0 & T_s & 1 \end{bmatrix} \quad (25)$$

The measurement matrix H is linear and constant:

$$H_k = \frac{\partial h(x)}{\partial x} = \begin{bmatrix} 1 & 0 & 0 & 0 \\ 0 & 1 & 0 & 0 \end{bmatrix} \quad (26)$$

The matrix F_k is derived analytically from the PMSM model and depends on $\hat{\omega}_e$ and $\hat{\theta}_e$, which makes the EKF adaptive to operating conditions.

The EKF algorithm operates in a closed-loop recursive configuration, integrating the nonlinear model with measurement feedback through two principal stages:

Prediction Stage: The algorithm projects the state and error covariance ahead

- State vector prediction:

$$\hat{x}_{k|k-1} = f\left(\hat{x}_{k-1|k-1}, u_{k-1}\right) \quad (27)$$

- Prediction error covariance matrix:

$$P_{k|k-1} = F_k P_{k-1|k-1} F_k^T + Q \quad (28)$$

Correction Stage: The predicted estimates are updated using actual measurements

- Update:

$$\tilde{y}_k = y_k - h\left(\hat{x}_{k|k-1}\right) \quad (29)$$

- Kalman-gain calculation:

$$K_k = P_{k|k-1} H_k^T (H_k P_{k|k-1} H_k^T + R)^{-1} \quad (30)$$

- State-estimate correction:

$$\hat{x}_{k|k} = \hat{x}_{k|k-1} + K_k \tilde{y}_k \quad (31)$$

- Covariance update:

$$P_{k|k} = \left(I - K_k H_k\right) P_{k|k-1} \quad (32)$$

The convergence and tracking performance of the EKF are strictly governed by the stochastic properties of the process-noise covariance matrix Q and the measurement-noise covariance matrix R. In this design, Q represents the uncertainties in the motor model and discretization process, while R characterizes the noise levels of the current acquisition system.

For the simulated PMSM drive, the covariance matrices are tuned as follows:

- Process-noise covariance matrix (Q): To ensure a high degree of responsiveness to speed transients while suppressing estimation ripples, the diagonal elements are assigned as:

$$Q = \mathrm{diag}\left([10^{-3}, 10^{-3}, 1, 10^{-4}]\right) \quad (33)$$

- Measurement-noise covariance matrix (R): Given the resolution of the current sensors and the signal-to-noise ratio (SNR) in the $\alpha-\beta$ frame, R is chosen as:

$$R = \mathrm{diag}\left([2.6\times10^{-3}, 4\times10^{-3}]\right) \quad (34)$$

The optimized ratio between Q and R ensures that the Kalman gain K yields a fast dynamic response without compromising the steady-state accuracy, which is crucial for high-performance sensorless FOC.

IV. Results and Discussion

The four sensorless speed-estimation methods are evaluated by simulation using the PMSM parameters in Table I. The test profile was selected to examine both transient and steady-state behavior: the speed command changes from 500 rpm to 1000 rpm at t = 0.5 s, then to 1500 rpm at t = 1 s. The simulation also includes sudden load-torque disturbances of 5 N.m and 10 N.m so that the tracking capability and disturbance rejection of each observer can be compared under the same operating conditions.

TABLE I. Parameters Used in Simulation

No.	Parameter	Value	Unit
1	Stator resistance (R_s)	0.129	Ohm
2	Stator d-axis inductance (L_{sd}))	0.0054	H
3	Stator q-axis inductance (L_{sq})	0.0054	H
4	Permanent magnet flux linkage (ψ_f)	0.1821	Wb
5	Number of pole pairs (p)	4	pairs
6	Rotor inertia (J)	0.003334	kg/m^2
7	Friction coefficient (B)	0.000425	Nms/rad
8	DC-Link voltage (V_{dc})	300	V

Figure 6 compares the actual rotor speed response and the speeds estimated by the SMO, LO, EKF, and MRAS observers; the reference speed is included only as a benchmark for the imposed operating profile. All four observers are able to follow the speed variations, but their transient behavior is clearly different. The EKF gives the closest speed reconstruction and the smallest overshoot during acceleration, whereas the SMO exhibits small high-frequency oscillations caused by the switching nature of the observer. The LO provides a smoother waveform than the SMO but shows a noticeable transient deviation when the operating point changes rapidly. The MRAS has the largest oscillation during the initial transient and during speed transitions because its adaptation mechanism requires additional time to converge. These observations are consistent with the quantitative results in Table II, where the EKF achieves the lowest speed RMSE of 1.24 rpm and the lowest steady-state error of 0.05%, while the MRAS has the

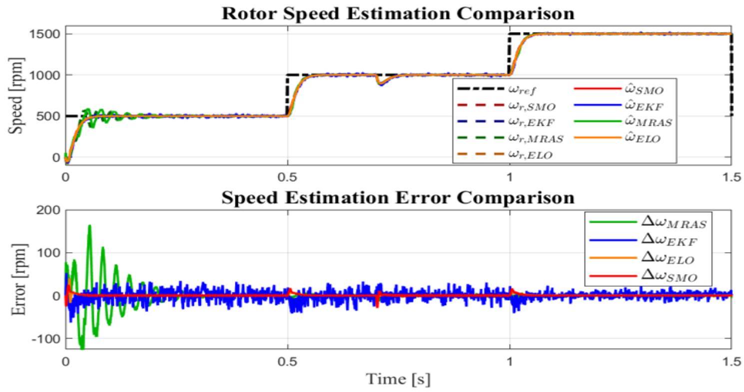

Fig. 6. Comparison of actual rotor speed and estimated speeds obtained by SMO, LO, EKF, and MRAS

highest speed RMSE of 3.87 rpm.

TABLE II. QUANTITATIVE PERFORMANCE COMPARISON

Criteria	SMO	LO	EKF	MRAS
Speed RMSE (rpm)	2.84	3.42	1.24	3.87
Position RMSE (rad)	0.035	0.048	0.014	0.055
Steady-state Error (%)	0.12	0.18	0.05	0.25
Max. Transient Error (rpm)	28.5	42.6	16.4	35.2

The rotor-angle estimation results in Fig. 7 further confirm the different dynamic characteristics of the observers. The EKF reconstructs the sawtooth angle waveform with the smallest error band, leading to the lowest position RMSE of 0.014 rad in Table II. The SMO and LO maintain bounded angle errors, although the LO shows a slight phase delay during high-speed operation. The MRAS angle estimate is more sensitive during transients, particularly at the beginning of the simulation. In addition, the d-q current responses in Fig. 8 provide an independent view of the control quality. The q-axis current follows the torque-producing demand during speed changes and load disturbances, whereas the d-axis current should remain close to its reference. The EKF and LO produce relatively smooth current responses, while the MRAS shows larger oscillations, especially in the d-axis current after the speed steps. This added result demonstrates that observer performance affects not only the estimated speed and angle but also the current-loop behavior of the sensorless drive.

The additional current-response and spectral analyses strengthen the comparison by showing how the estimation methods influence the closed-loop PMSM drive beyond the speed waveform. Table III summarizes the qualitative trade-offs. The EKF offers the best estimation accuracy and noise attenuation, the SMO provides strong robustness to load disturbances, and the LO and MRAS remain attractive for low-cost implementations because of their simpler structures.

TABLE III. COMPARISON OF CONTROL QUALITY OF METHODS

Criteria	SMO	LO	EKF	MRAS
Dynamic Response	Fast	Moderate	Excellent	Fast
Noise Immunity	Moderate	Moderate	Excellent	Low
Robustness	High	Medium	Medium	Low
Computational Cost	Medium	Low	Very High	Low
Implementation	Moderate	Simple	Complex	Simple

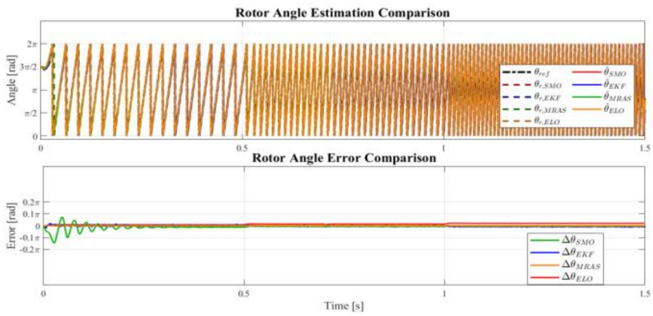

Fig. 7. Comparison of actual rotor angle and estimated angle obtained by SMO, LO, EKF, and MRAS

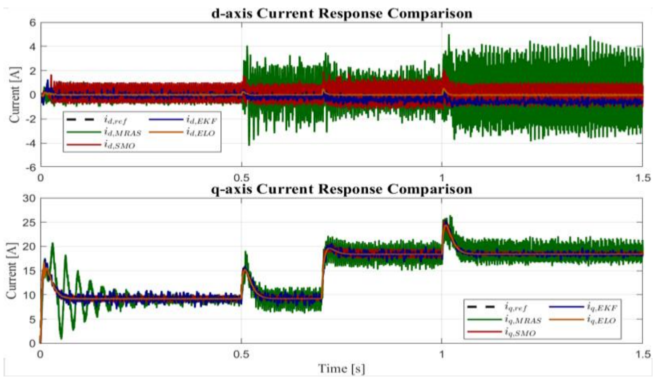

Fig. 8. Comparison of dq-axis current response obtained by SMO, LO, EKF, and MRAS

Figure 9 presents the current THD comparison, which provides additional information that cannot be directly inferred from the speed and angle waveforms alone. The THD values were obtained from the frequency spectrum of the analyzed current signal under the same steady-state operating condition. This metric is used to evaluate the harmonic content associated with each estimation method and its influence on the closed-loop current response. The LO and MRAS produce the lowest THD values of about 1.36%, whereas the EKF and SMO show higher harmonic contents of about 6.47% and 6.65%, respectively. This result should be interpreted together with Table II: although the MRAS has low harmonic content in the frequency-domain result, it still suffers from larger transient speed and position errors. Conversely, the EKF provides the best overall estimation accuracy and disturbance rejection, but this advantage is obtained at the expense of higher computational complexity and a higher THD level in the analyzed signal. Therefore, the additional simulations clarify the practical trade-off among estimation accuracy, transient response, harmonic content, robustness, and implementation cost.

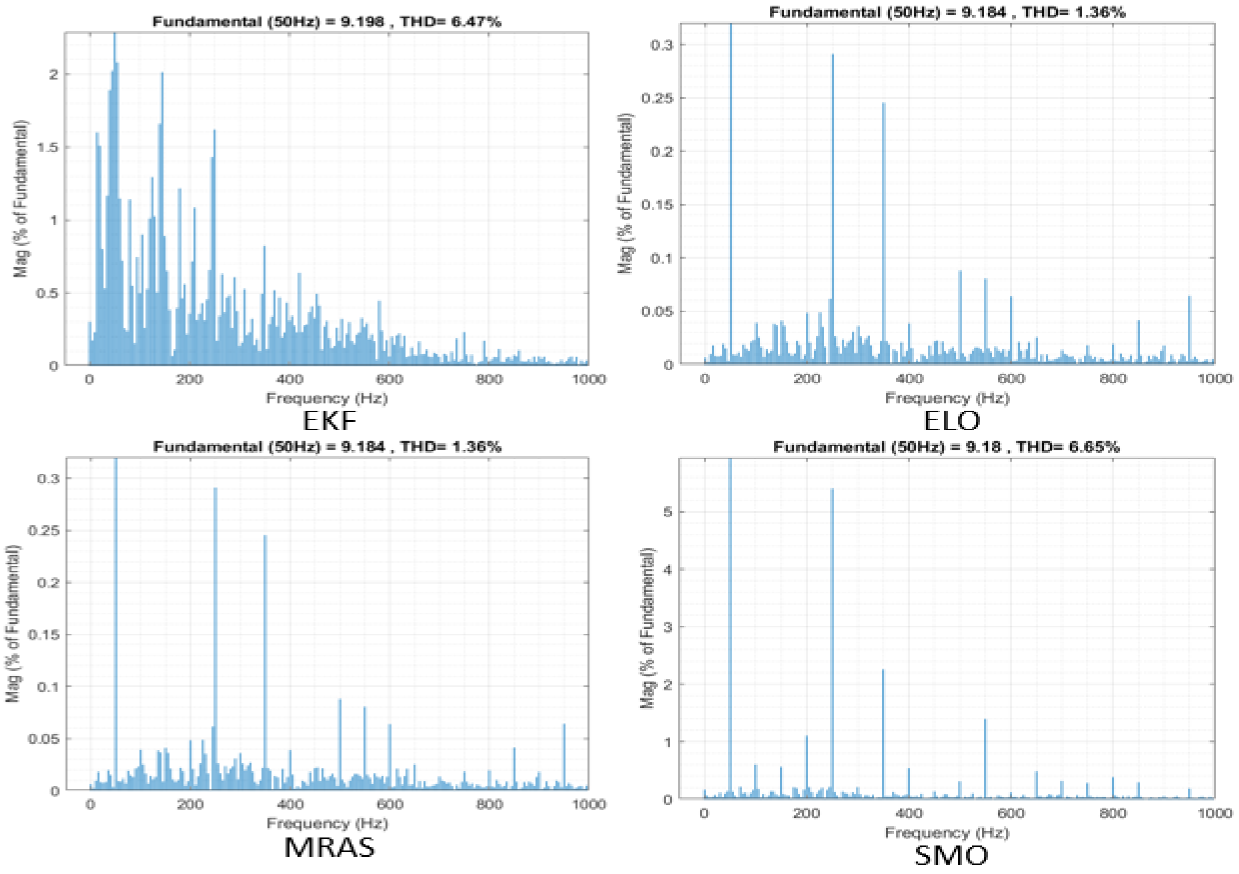

Fig. 9. Current THD comparison of SMO, LO, EKF, and MRAS

V. CONCLUSION

This paper presented a unified comparative evaluation of four representative model-based sensorless speed-estimation methods for PMSM drives, namely the Luenberger observer, sliding-mode observer, model reference adaptive system, and extended Kalman filter. All observers were implemented under the same PMSM parameters, speed/load profile, and simulation conditions to ensure a fair comparison. The evaluation was not limited to speed tracking, but was extended to rotor-position estimation, current behavior, THD, steady-state error, transient response, disturbance rejection, and implementation complexity.

The obtained results show that the EKF provided the best overall estimation accuracy among the four evaluated methods. It achieved the lowest speed RMSE of 1.24 rpm, position RMSE of 0.014 rad, steady-state speed error of 0.05%, and maximum transient speed error of 16.4 rpm. These quantitative results confirm that the EKF is the most suitable option when high estimation accuracy is the primary requirement. However, this improvement is achieved at the expense of higher computational burden and a more complex implementation structure, which should be carefully considered in real-time embedded motor-drive applications.

The SMO demonstrated strong disturbance-rejection capability and maintained acceptable speed-estimation performance during load variations. Nevertheless, its switching nature introduced visible high-frequency oscillations in the estimated response, which may affect current-loop smoothness and increase harmonic components. The LO showed a simpler structure and smoother current response, making it attractive for applications requiring moderate accuracy and low implementation complexity. The MRAS exhibited a relatively low THD value, but it produced larger transient speed and position errors compared with the EKF and SMO. This indicates that low harmonic distortion alone is not sufficient to guarantee superior overall estimation performance.

Therefore, the main finding of this study is that the selection of a sensorless estimator for PMSM drives should not be based on a single criterion. Instead, it requires a combined assessment of estimation accuracy, transient behavior, current-response quality, harmonic distortion, disturbance robustness, and computational cost. Under the considered simulation conditions, the EKF is recommended for accuracy-oriented applications, the SMO is suitable for systems requiring strong robustness, while the LO and MRAS can be considered for lower-complexity implementations. Future work will focus on real-time validation of the comparative results on an FPGA-based PMSM drive platform to further evaluate computational feasibility and practical applicability.

REFERENCES

[1] Y. Xu, M. Yao, and X. Sun, “Overview of Position-Sensorless Technology for Permanent Magnet Synchronous Motor Systems,”

World Electric Vehicle Journal, vol. 14, no. 8, p. 212, 2023, doi: 10.3390/wevj14080212.

[2] Y. Ran, M. Qiao, L. Sun, and Y. Xia, “Review of Position Sensorless Control Technology for Permanent Magnet Synchronous Motors,” Energies, vol. 18, no. 9, p. 2302, 2025, doi: 10.3390/en18092302.

[3] P. Brandstetter, P. Rech, and P. Simonik, “Sensorless Control of Permanent Magnet Synchronous Motor Using Luenberger Observer,” in PIERS Proceedings, Cambridge, USA, 2010.

[4] O. M. Arafa, G. A. Abdel Aziz, M. I. Abu El-Sebah, and A. A. Mansour, “Observer-based sensorless speed control of PMSM: A focus on drive’s startup,” Journal of Electrical Systems and Information Technology, vol. 3, pp. 181–209, 2016, doi: 10.1016/j.jesit.2015.05.004.

[5] R. Luo, Z. Wang, and Y. Sun, “Optimized Luenberger Observer-Based PMSM Sensorless Control by PSO,” Modelling and Simulation in Engineering, vol. 2022, Article ID 3328719, 2022, doi: 10.1155/2022/3328719.

[6] H. M. Kojabadi and M. Ghribi, “MRAS-based Adaptive Speed Estimator in PMSM Drives,” in Proc. 2006 9th IEEE International Workshop on Advanced Motion Control, 2006, pp. 569–572, doi: 10.1109/AMC.2006.1631722.

[7] A. Khlaief, M. Boussak, and A. Chaari, “A MRAS-based stator resistance and speed estimation for sensorless vector controlled IPMSM drive,” Electric Power Systems Research, vol. 108, pp. 1–15, 2014, doi: 10.1016/j.epsr.2013.09.018.

[8] B. Bendjedia and S. Chouireb, “Comparative Study Between Sensorless Vector Control of PMSM Drives based on MRAS, SMO and EKF Observers,” in Proc. 2023 International Conference on Advances in Electronics, Control and Communication Systems (ICAECCS), 2023, doi: 10.1109/ICAECCS56710.2023.10104927.

[9] G. Ram and S. K. R., “Review of Sliding Mode Observers for Sensorless Control of Permanent Magnet Synchronous Motor Drives,” International Journal of Power Electronics and Drive Systems (IJPEDS), vol. 9, no. 1, pp. 46–54, 2018, doi: 10.11591/ijpeds.v9.i1.pp46-54.

[10] S. Ye, “Fuzzy sliding mode observer with dual SOGI-FLL in sensorless control of PMSM drives,” ISA Transactions, vol. 85, pp. 161–176, 2019, doi: 10.1016/j.isatra.2018.10.004.

[11] S. Ye, “Design and performance analysis of an iterative flux sliding-mode observer for the sensorless control of PMSM drives,” ISA Transactions, vol. 94, pp. 255–264, 2019, doi: 10.1016/j.isatra.2019.04.009.

[12] S. Ye and X. Yao, “A Modified Flux Sliding-Mode Observer for the Sensorless Control of PMSMs With Online Stator Resistance and Inductance Estimation,” IEEE Transactions on Power Electronics, vol. 35, no. 8, pp. 8652–8662, 2020.

[13] G. Wang and H. Zhang, “A new speed adaptive estimation method based on an improved flux sliding-mode observer for the sensorless control of PMSM drives,” ISA Transactions, vol. 128, pp. 675–685, 2022, doi: 10.1016/j.isatra.2021.09.003.

[14] Z. Zheng, Y. Li, and M. Fadel, “Sensorless control of PMSM based on extended Kalman filter,” in Proc. 2007 European Conference on Power Electronics and Applications (EPE), 2007, doi: 10.1109/EPE.2007.4417275.

[15] D. Janiszewski, “Extended Kalman Filter Based Speed Sensorless PMSM Control with Load Reconstruction,” in Proc. IECON 2006 - 32nd Annual Conference on IEEE Industrial Electronics, 2006, doi: 10.1109/IECON.2006.347852.